ACTA TECHNICA JAURINENSIS
Vol. XX, No. Y, pp. ZZ-ZZ, 2026
10.14513/actatechjaur.00875

Research Article

Determination of rail dilatation movements at tunnel gates for ballasted railway tracks in case of a greater change of temperature

Nándor Liegner[1], Szabolcs Fischer[2,*]

[1]Department of Highway and Railway Engineering, Faculty of Civil Engineering, Budapest University of Technology and Economics
Műegyetem rakpart 3, Budapest, 1111, Hungary
[2]Department of Transport Infrastructure and Water Resources Engineering, Faculty of Architecture, Civil and Transport Engineering, Széchenyi István University
Egyetem tér 1, Győr, 9026, Hungary
*e-mail: fischersz@sze.hu

Submitted: 23/01/2026 *Revised: 20/04/2026* *Accepted: 22/04/2026* *Published online: 26/04/2026*

Abstract: The temperature change in continuously welded rail (CWR) tracks induces substantial internal stresses and shifts sleeper positions because the rails are longitudinally restrained from thermal expansion. This phenomenon is significantly intensified at tunnel portals, where a sharp contrast exists between the thermal boundary conditions of the open track and those of the sheltered tunnel environment. The current article investigates the dynamic interplay between rail dilatation and axial forces at these critical junctions by employing a finite-element (FE) model of the 54E1 rail track, calibrated using experimental measurements of track fastening parameters and ballast behavior. The research specifically examines the combined influence of temperature gradients between the tunnel and open environments, the bilinear longitudinal resistance of the ballast, and the mechanical braking loads exerted by passing trains. Through a series of parametric studies, the results demonstrate that simultaneous thermal and braking forces can trigger extreme rail displacements of up to 100 mm and axial forces of up to 1.4 MN. Notably, such high-stress states occur even when the ballast resistance is only 7 N/mm lower than the braking force. While increasing track fastening resistance helps equalize the impact of braking and thermal effects, it effectively reduces deflections to non-critical levels. The most severe stability risks are identified when the center of the braking zone aligns precisely with the portal. Ultimately, the study concludes that ballast resistance is the decisive factor in managing track integrity at tunnel entrances.

Keywords: railway track; CWR track; track-tunnel interaction; change of temperature; thermal force; thermal expansion

I. INTRODUCTION

Continuously welded rail (CWR) tracks are widely used in modern railway systems because they provide smoother operation, lower maintenance needs, and improved overall performance. At the same time, the absence of rail joints means the rails cannot expand or contract freely with temperature changes. Instead, thermal expansion is restrained by the rail-fastener-sleeper–ballast system, resulting in longitudinal forces in the rail. These forces play an important role in determining the mechanical behavior and safety of the track.

As rail temperature increases, compressive forces develop and may lead to track misalignment or buckling, while lower temperatures generate tensile forces that increase the risk of rail fracture. The magnitude of these forces depends not only on the temperature change itself but also on the track's resistance characteristics and the actual operating conditions. Transition zones, such as tunnel portals, are especially critical in this regard. In these locations, the thermal conditions of the open track and the tunnel interior can differ significantly, leading to localized rail movements and changes in internal forces. These effects can become even more pronounced when thermal loads interact with operational influences such as braking and

acceleration. For this reason, a detailed understanding of the combined effects of temperature variation, track resistance, and operational loads is essential for ensuring the safe and reliable performance of CWR tracks.

1. Longitudinal Ballast Resistance Based on Hungarian Literature

According to the Hungarian railway regulation, MÁV Zrt. D.12/H [1] (MÁV Zrt. means Hungarian State Railways Ltd.), which governs the design, construction, and maintenance of continuously welded rail (CWR) tracks, the nominal stress-free (neutral) temperature of the rail is defined as 23 °C, with an allowable neutral temperature range specified in the standard [1]. In service, however, rail temperatures can vary over a much wider interval. Under strong solar radiation, rail temperatures may reach approximately 60 °C during summer, while significantly lower values may occur in winter. Although a minimum temperature of –30 °C is typically considered in design, long-term observations indicate that such extreme values are rarely reached under actual climatic conditions in Hungary [1].

Hungarian technical literature provides commonly accepted values for the longitudinal resistance of ballasted tracks. For newly constructed and properly compacted ballast, the longitudinal resistance per unit length of track is typically taken as approximately p = 5 N/mm. As the track is subjected to repeated loading and consolidates under traffic, its resistance increases, generally reaching 8–10 N/mm. In the case of frozen ballast, the resistance may increase further, potentially reaching 10-20 N/mm due to the increased stiffness of the ballast layer [2]. These characteristic values are widely used in engineering practice and serve as a basis for estimating the track's longitudinal behavior.

The relationship between longitudinal ballast resistance and rail displacement has been studied in detail by Nemesdy, who developed both exact and simplified approaches for analyzing the restrained thermal expansion of CWR tracks [3]. Experimental observations show that ballast resistance is a nonlinear function of displacement, typically consisting of an initial elastic response followed by a plastic phase in which the resistance reaches a limiting value. **Fig. 1** illustrates typical representations of this behavior. **Fig. 1(a)** shows an example of a measured resistance-displacement relationship, while **Fig. 1(b)** and **Fig. 1(c)** present bilinear idealizations of the ballast behavior. **Fig. 1(d)** shows a simplified approach in which the longitudinal resistance is assumed constant.

In engineering practice, bilinear models are frequently used because they provide a reasonable balance between accuracy and simplicity, allowing both the elastic stiffness and the limiting resistance of the ballast to be considered. In contrast, assuming a constant resistance simplifies calculations but neglects the nonlinear characteristics of the ballast response. In this study, the bilinear representation shown in **Fig. 1(c)** is adopted for the numerical modeling.

2. Variation of Longitudinal Rail Restraint and Ballast Resistance According to Standards

The longitudinal resistance of the track is governed by the combined behavior of the rail fastenings and the ballast, both of which contribute to the restraint of rail movement. International standards and technical guidelines provide recommendations for these resistance components; however, the values are often dependent on the specific track system and operating conditions.

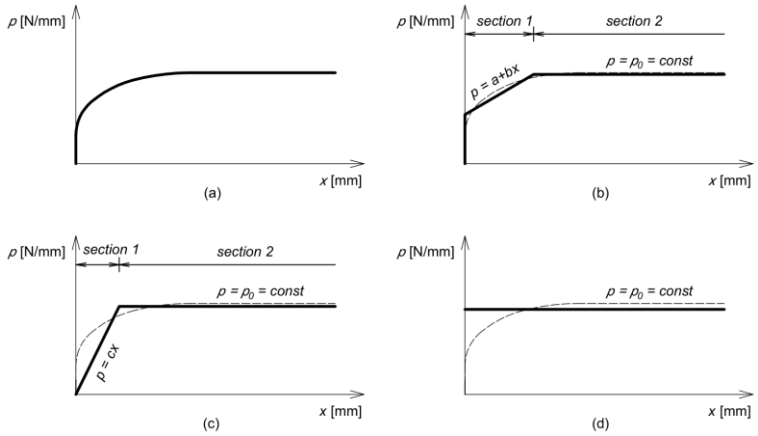

Figure 1. *Mathematical modelling possibilities of ballast resistance according to Nemesdy [3], (a) a possible test result, (b) bilinear approximation (I), (c) bilinear approximation (II), (d) approximation by a constant*

The European standard EN 1991-2:2003 [4] addresses the interaction between track and structures and provides general guidance on the stiffness and resistance of track components. It distinguishes between loaded and unloaded track conditions, indicating that the longitudinal restraint of rail fastenings under load can be significantly higher than in the unloaded state. However, the standard does not define fixed numerical values for these parameters, as they depend on the type of fastening system and track configuration.

More detailed numerical values are provided in technical literature. According to the handbook Track Installations [5], the longitudinal resistance of a loaded track can be approximated by considering the contributions of both the rail-sleeper connection and the sleeper-ballast interaction. For loaded conditions, a total longitudinal resistance of approximately 60 kN/m is suggested, which can be decomposed into about 30 kN/m for the rail fastening and about 20 kN/m for the ballast, with the remaining portion attributed to additional interaction effects. In the unloaded state, lower values are typically assumed, with approximately 30 kN/m for the fastening system and 20 kN/m for the ballast [5].

Recommendations are also provided by UIC Code 774-3, which focuses on track-bridge interaction [6]. This guideline differentiates between maintenance conditions and loading states. For unloaded tracks, the longitudinal resistance of sleepers in ballast is typically taken as approximately 12 kN/m for moderately maintained tracks and about 20 kN/m for well-maintained tracks. Under loaded conditions, or in the presence of frozen ballast, the resistance may increase significantly, with values up to 60 kN/m being recommended [6].

These references highlight that the longitudinal resistance of the track is not a fixed parameter but depends on several factors, including the fastening system, ballast condition, maintenance level, and the presence of vertical loads. As a result, selecting appropriate resistance values is an important aspect of track modeling and significantly influences the predicted longitudinal behavior of the rail.

3. General International Literature Overview

In CWR tracks, rails are restrained by the rail-fastener-sleeper-ballast system, so temperature changes generate longitudinal resistance forces and axial stresses. Classical railway engineering formulations describe the equilibrium of a rail element under temperature variation [7]. Heating produces compressive forces that may lead to track misalignment or buckling, while cooling induces tensile forces that increase the risk of rail fracture; this dual risk is a fundamental safety concern in CWR systems [8].

Thermal stresses depend strongly on the rail temperature field. Measurements show that both longitudinal temperature variation and cross-sectional temperature gradients significantly influence stress distribution [9]. Environmental factors such as solar radiation, cloud cover, vegetation, and terrain affect temperature profiles along the track [9]. Thermal imaging and field measurements have identified temperature differences as indicators of buckling-prone sections [10]. Laboratory and field studies indicate that cross-sectional temperature differences may exceed 6–7 °C, demonstrating that the assumption of uniform temperature may introduce inaccuracies [11,12].

Longitudinal rail stresses are also influenced by additional mechanisms, including rail creep, non-uniform resistance distribution, and structural interactions such as bridge expansion [13]. These effects can induce transverse and vertical stresses due to the Poisson effect. Variations in stress-free temperature along the track and over time have been observed, with daily fluctuations of several degrees Celsius [14,15]. Accurate stress evaluation is essential for maintenance planning, as both buckling and rail breakage pose derailment risks [16]. Moreover, braking and acceleration forces interact with thermal effects, influencing longitudinal behavior [17].

Track behavior is further affected by vehicle-track interaction. Vehicle dynamics, suspension characteristics, and operating conditions influence the transmission of loads into the track structure [18–20]. Multibody system (MBS) approaches are widely used to analyze these interactions and complement structural and thermal modeling [21].

Recent studies emphasize system-level modeling and optimization in transport engineering. Multimodal transport optimization, scheduling, and decision-making methods demonstrate that infrastructure loading conditions are also influenced by operational strategies and uncertainties [22–24]. Improvements in logistics and braking processes can modify longitudinal force development in the track [23,25]. These findings highlight the importance of integrating mechanical and operational perspectives in railway engineering.

Tunnel portals represent critical transition zones due to differences in thermal boundary conditions between the open track and the tunnel interior. While open tracks experience large temperature variations, tunnels provide more stable conditions, leading to steep thermal gradients near portals [26]. Monitoring studies confirm that temperature-induced deformations are more pronounced in portal regions than in deeper tunnel sections [27,28]. These gradients cause localized rail displacements and force redistribution, making tunnel gates particularly sensitive zones.

The mechanical response of rails under thermal loading can be described by restrained thermal strain, in which the axial force depends on the temperature change, the thermal expansion coefficient, and material properties [29]. Analytical and numerical models represent ballast, sleepers, and fastenings to simulate track behavior. These models show that stability depends on temperature, resistance characteristics, imperfections, and boundary conditions [30–32]. In curved tracks, thermal forces may also generate lateral components [33].

Track resistance plays a key role in controlling rail movements. Ballast-sleeper interaction provides longitudinal, lateral, and vertical resistance components [34]. Experimental and field studies show that resistance depends on ballast condition, vertical load, fastening systems, and measurement methods [35–39]. Additional research highlights the contributions of sleepers and fastenings, the influence of vertical loading [40,41], and variability across different sleeper types [42]. Field investigations confirm that resistance varies under real operating conditions [43].

Ballast condition and geometry significantly affect stability. Degradation and fouling reduce resistance and increase susceptibility to buckling [44,45]. Crib ballast often contributes most to longitudinal resistance [35], while fastening systems exhibit nonlinear behavior influenced by clamping force and vertical loading [46]. Accurate modeling, therefore, requires detailed characterization of resistance properties, especially in transition zones.

Vertical track stiffness and its spatial variability also influence longitudinal behavior by modifying load transfer and force distribution [47–49]. At tunnel portals, stiffness discontinuities may further complicate track response. Additionally, rail welding can introduce residual stresses affecting thermal behavior [50].

Accurate prediction of rail behavior requires integrating thermal loading, resistance characteristics, and structural response. Analytical and numerical models for thermal buckling incorporate nonlinear ballast behavior, imperfections, and dynamic loading [30–32], but require validation through measurements.

Measurement techniques are essential for assessing thermal effects in CWR. Conventional temperature measurements may be inaccurate due to environmental influences [51], whereas modern monitoring systems use integrated sensors and data analysis to enable predictive maintenance [52]. Strain-based systems and distributed fiber-optic sensing enable continuous monitoring of rail stress and temperature with high spatial resolution, making them suitable for transition zones such as tunnel portals [12,53,54]. Data-driven approaches can also detect unexpected behavior during maintenance [55].

Climate change increases the frequency of high-temperature events, increasing buckling risk and operational restrictions [56]. Maintenance activities, such as ballast renewal, can alter resistance and induce rail displacements [57].

Various engineering solutions have been proposed to improve track performance. Under-ballast mats and under-sleeper pads modify stiffness and damping [58,59], while ground improvement techniques and resilient inclusions affect track behavior in stiff subgrades [60]. Polyurethane reinforcement has also been investigated to enhance stability [61].

Despite extensive research, the combined effects of temperature variation, resistance characteristics, and structural transitions at tunnel portals remain complex and not fully understood [62–64]. Many analyses rely on simplifying assumptions, such as uniform temperature and constant resistance, even though real conditions are more complex. Therefore, advanced modeling and monitoring are required to accurately describe rail behavior in critical zones such as tunnel gates.

4. Identification of the Research Gap, Novelty of the Current Paper

The literature shows that the behavior of CWR tracks under temperature effects has been widely studied. It is well known that changes in rail temperature relative to the neutral temperature generate longitudinal forces in the rail, which are resisted by the rail-fastener-sleeper-ballast system. These forces lead to compression at high temperatures and tension at low temperatures, both of which represent significant safety risks, as they may result in track buckling or rail fracture.

Previous studies have also demonstrated that the magnitude of these forces depends strongly on the track structure's resistance characteristics. Several factors, including ballast condition, maintenance level, fastening systems, and vertical loading, influence longitudinal resistance. As presented in Sections I.1 and I.2, both national guidelines and international standards provide characteristic values for ballast resistance and rail restraint. However, these values are often idealized; in practice, resistance can vary considerably depending on the actual track condition.

Another important aspect highlighted in the literature is that rail temperature is rarely uniform. Both longitudinal temperature variation along the track and temperature differences within the rail cross-section have been observed. These variations are influenced by environmental conditions such as solar radiation, shading, and local terrain. In this

context, transition zones play a particularly important role. At tunnel portals, the thermal conditions of the open track and the tunnel interior differ significantly, leading to steep temperature gradients. As a result, localized rail displacements and changes in internal forces may occur in these regions.

In addition to thermal effects, the longitudinal behavior of the track is also influenced by operational loads. Braking and acceleration forces, as well as vehicle-track interaction, generate additional longitudinal forces in the rail. Although these effects have been investigated in the literature, they are often treated separately from thermal loading, and their combined influence is usually simplified in practical analyses.

Despite the extensive research available, several limitations can be identified. Many studies assume uniform temperature distribution, constant resistance characteristics, or simplified loading conditions. In particular, the combined effects of significant temperature differences at tunnel portals, realistic ballast resistance behavior, and operational loads have not yet been fully clarified. The interaction between unloaded and loaded track conditions, which affects both resistance and displacement, is also often neglected.

Therefore, a more detailed investigation of rail behavior in transition zones, especially at tunnel gates where thermal and mechanical conditions change abruptly, is required. To address this need, the study numerically analyzes rail dilatation movements and internal forces in ballasted CWR tracks by jointly considering tunnel-open track temperature differences, realistic bilinear ballast resistance, and braking forces, showing that the most critical responses occur when braking zones coincide with portal thermal discontinuities and identifying ballast resistance thresholds beyond which braking effects become negligible.

This paper is organized as follows. Section II describes the laboratory and field tests used to determine the key resistance characteristics of the track. Section III outlines the numerical modeling approach, including the main assumptions and loading conditions applied in the analysis. Sections IV through VII present the results for different ballast resistance levels and examine the effects of temperature changes and braking forces, both separately and in combination. Finally, Section VIII summarizes the main findings and highlights the key conclusions regarding rail behavior at tunnel portals under varying thermal and operational conditions.

II. Laboratory and Field Tests

The mechanical properties of the track components used in numerical analysis were determined through laboratory and field investigations. In particular, the longitudinal restraint of the rail fastenings, as well as the lateral and longitudinal resistance of the ballast, were evaluated to provide realistic input parameters for the modeling.

The longitudinal rail restraint of the W14 fastening system was measured in the Track Laboratory of the Department of Highway and Railway Engineering at the Budapest University of Technology and Economics, in accordance with the requirements of EN 13146-1:2019 [65]. The tests were conducted under controlled laboratory conditions, yielding an average longitudinal restraint of 11.06 kN for the fastening system [26]. Additional experimental investigations on the longitudinal behavior of rail fastenings, including the Vossloh Skl 12 system, have also been conducted in the same laboratory, and the results have been reported in earlier publications [66].

The lateral resistance of the ballast was determined using a full-scale track panel test. A test section consisting of four LM-type prestressed concrete sleepers, two rails, and W14 fastening systems was constructed in a prepared ballast bed. The ballast shoulder width was set to 0.45 m. During the test, lateral loads were applied to the track panel, and the resulting displacements were measured. The maximum lateral resistance per unit length of track was found to be 7.54 N/mm, while 7.39 N/mm was obtained at a lateral displacement of 2 mm [26].

The longitudinal resistance of the ballast was also investigated using a similar track panel configuration. The test section consisted of four LM-type concrete sleepers, K (Geo) fastening systems, and two rails installed in a ballast bed with a shoulder width of 0.40 m. The ballast was compacted using petrol-driven vibrators to achieve representative in-situ conditions. The measured longitudinal resistance of the track panel ranged between 5.3 kN and 5.9 kN for compacted but not yet fully consolidated ballast [26].

The results of these laboratory and field tests provide representative values for the track structure's resistance characteristics. These parameters serve as input to the numerical model presented in the following sections, ensuring that the simulations reflect realistic track behavior under thermal and operational loading conditions.

III. General Structure of the Computation Model

In this section, the authors introduce the calculation methods considered, the developed and applied finite element model, the types of supports, and the assigned loads.

1. Basic Concepts, Supports

For the purposes of this study, a numerical model was developed using the finite element software AxisVM X5. The railway superstructure was represented by a two-dimensional model corresponding to one half of the track cross-section. The rails were modeled as line-supported Euler-Bernoulli beam elements, with mechanical properties consistent with the 54E1 rail profile [26,67].

The analysis assumes a continuously welded rail (CWR) track without the use of rail expansion devices at the tunnel portals. Only straight track sections are considered, and lateral stability is assumed to be ensured. Although lateral stability may become a critical issue in curved tracks, this aspect is outside the scope of the present study and is not addressed here.

The longitudinal resistance of the ballast depends strongly on its condition and the level of consolidation. For newly constructed ballast, a typical value of approximately 5 N/mm per rail can be assumed, whereas well-maintained, consolidated ballast under traffic conditions may exhibit resistance values of 8–10 N/mm. Under the influence of vertical loads from passing trains, the effective longitudinal resistance increases further and can reach approximately two to three times the value of unloaded ballast, i.e., about 10–15 N/mm.

To investigate the influence of ballast resistance on track behavior, a sensitivity analysis was performed. Three different cases were considered, representing varying resistance levels of the ballast under operational conditions [26]:

- the longitudinal ballast resistance is 7 N/mm, that is less than the braking load;
- the longitudinal ballast resistance is 10 N/mm, that is equal to the braking load;
- the longitudinal ballast resistance is 15 N/mm, which is greater than the braking load.

For support, a bilinear elastic-plastic stiffness has been assumed, as shown in **Fig. 1(c)**. Within the elastic part, the longitudinal stiffness has been assumed on the basis that the maximum longitudinal load per rail is 4.8 kN, the elastic displacement of the ballast is 1 mm, the sleeper spacing is 0.6 m, and it will result in 4.8 (kN) / 1 mm / 0.6 m = 8 kN/mm/m in the unloaded models. In the case of the loaded models, the longitudinal elasticity has been taken to

- 8 / 5 × 7 = 11.2 kN/mm/m in case of a ballast resistance of 7 N/mm;
- 8 / 5 × 10 = 16.0 kN/mm/m in case of a ballast resistance of 10 N/mm;
- 8 / 5 × 15 = 24.0 kN/mm/m in case of a ballast resistance of 15 N/mm.

2. Considered Loads

Dilatation movements and longitudinal internal forces in a railway superstructure result from two main effects:

- change of temperature in the rail;
- braking and acceleration of the trains.

A. Change of Temperature in the Rail

The longitudinal response of CWR tracks is strongly influenced by temperature changes relative to the stress-free (neutral) temperature. According to Hungarian railway regulations (MÁV Zrt. D.12/H [1]), the nominal neutral temperature of the rail is specified as 23 °C, with an allowable tolerance range defined in the standard.

Deviations from this reference state generate axial forces and corresponding longitudinal displacements in the rail.

The thermal environment of railway tracks located in tunnels differs markedly from that of open-track sections. In tunnels, the absence of direct solar radiation and the thermal inertia of the surrounding ground lead to more stable temperature conditions. Consequently, temperature fluctuations inside the tunnel are generally smaller than those experienced by tracks on earthworks. The magnitude of this difference depends primarily on tunnel length: shorter tunnels tend to exhibit temperatures closer to ambient conditions, whereas longer tunnels maintain relatively constant temperatures throughout the year.

To capture the influence of these varying thermal conditions, a parametric analysis was performed using two representative scenarios. These scenarios describe different tunnel characteristics in terms of temperature behavior:

- Case' A' represents a medium-long tunnel; and
- Case' B' models a long tunnel with respect to temperature conditions.

In Case 'A', the rail temperature within the tunnel is assumed to vary between –5 °C in winter and +30 °C in summer. In contrast, the adjacent open-track section is subjected to a significantly wider temperature range, from –30 °C to +60 °C. Based on these assumptions, the effective temperature variation relative to a reference value of +28 °C is 33 °C inside the tunnel during winter and 58 °C on the open track. Under summer conditions, the corresponding temperature changes are 15 °C in the tunnel and 45 °C on the track section located on the earthworks [26,67].

Case 'B' represents a tunnel with more stable thermal conditions, where the rail temperature is assumed to vary between +15 °C in winter and +20 °C in summer. In this case, the resulting temperature change inside the tunnel is 13 °C during winter, while the open-track section experiences a 58 °C difference. During summer, the temperature change

is 5 °C within the tunnel and 45 °C on the earthworks. These assumptions reflect the reduced thermal variability typically observed in longer tunnels.

In the numerical model, the temperature field is represented as a discontinuous distribution at the tunnel portal. For example, under winter conditions, adjacent rail elements may be assigned temperatures of –30 °C and +15 °C. This approach provides a conservative representation of the thermal loading, as it introduces the maximum possible temperature gradient at the transition between the open track and the tunnel.

In practice, temperature variations occur gradually over a finite distance, influenced by factors such as tunnel length, atmospheric conditions, airflow, and heat exchange processes between the rail and its environment. A more realistic representation would involve a continuous temperature profile along the transition zone. Such an approach would allow for a sensitivity analysis to quantify the effect of the transition length on the resulting rail displacements and internal forces. However, the consideration of distributed temperature gradients is beyond the scope of the present study and is therefore identified as a subject for future research.

The modeling approach corresponding to Case 'A' has been presented and analyzed in detail in a previous publication by one of the authors [26]. The current study, however, focuses on Case 'B', which is intended to represent the thermal conditions of longer tunnels with limited temperature variation.

Throughout the analysis, the temperature is assumed to be uniform within each rail cross-section. As a result, potential temperature gradients across the rail profile are neglected, and only longitudinal temperature variations along the track are considered.

B. Braking and Acceleration Forces

According to EN 1991-2 (Eurocode 1) [4], braking actions on railway tracks can be represented by an equivalent uniformly distributed longitudinal load. The recommended characteristic value for braking is 20 kN/m, applied over a maximum total force of 6000 kN, corresponding to an effective loading length of 300 m.

Acceleration effects are also modeled as a uniformly distributed longitudinal load, typically taken as 33 kN/m per track, with an upper limit of 1000 kN.

Comparative assessments indicate that braking forces generally govern the longitudinal response of the track, as their magnitude and effects are significantly greater than those associated with acceleration [26,67].

C. Combination of Loads

The load cases considered in the analysis combine thermal effects (for both winter and summer conditions) with longitudinal braking forces applied over a 300 m track section. To identify the most unfavorable loading configurations, the position of the braking load was systematically varied along the track.

Specifically, the uniformly distributed braking load acting in the rightward direction was incrementally shifted in 50 m increments from the initial to the final positions illustrated in **Fig. 2(a)** and **Fig. 2(b)**, respectively. For braking in the opposite direction, equivalent load cases were generated by mirroring these positions.

Each braking load configuration was evaluated under both winter and summer temperature conditions, enabling a comprehensive assessment of the resulting internal forces and displacements under combined thermal and operational loading [26,67].

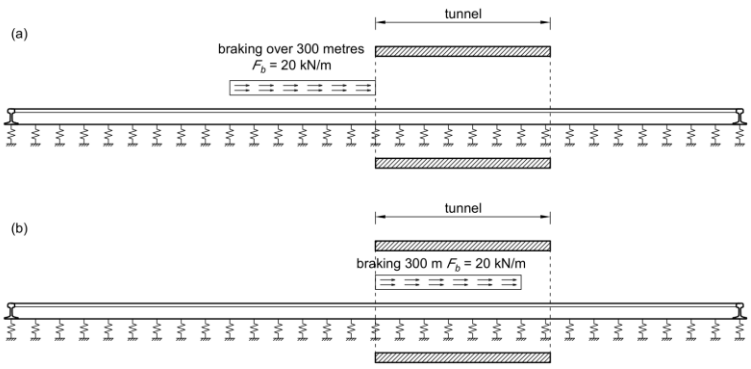

Figure 2. *Modeling the effect of braking, (a) starting position of braking, (b) end position of braking (at the bottom side, i.e., below the rails, there are supporting springs of continuous substituting beam*

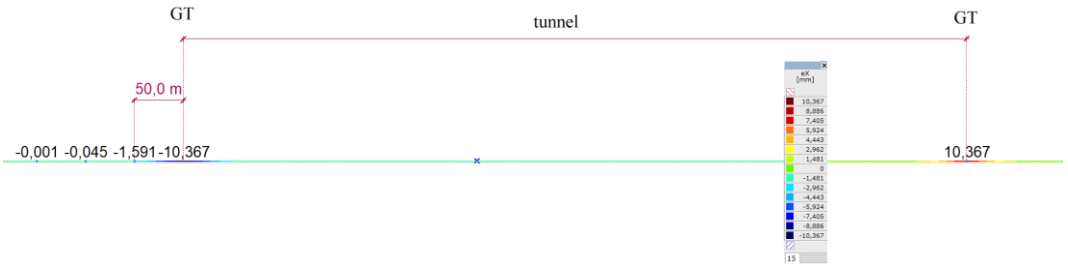

Figure 3. *Longitudinal displacement [mm] of the unloaded rail due to winter change of temperature (decimal commas are applied because of the original AxisVM X5 software)*

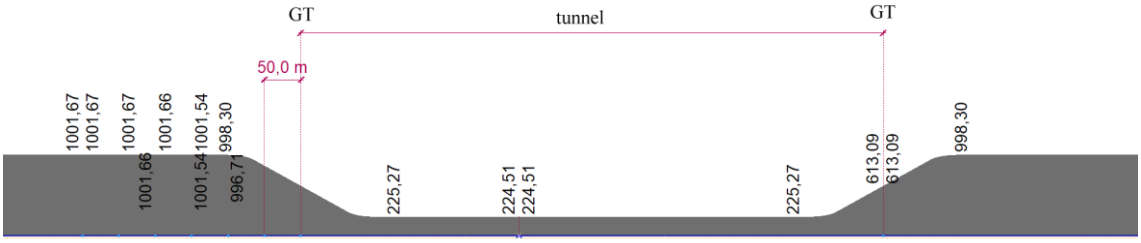

Figure 4. *Normal forces [kN] in the unloaded rail due to winter change of temperature (decimal commas are applied because of the original AxisVM X5 software)*

IV. Results of Internal Forces and Displacements from the Effects of Temperature Change, With the Assumption of a Ballast Resistance of p = 5 N/mm

From a mechanical perspective, the development of axial forces and longitudinal displacements in the rail due to thermal expansion can be regarded as a quasi-static process.

These temperature-induced effects are assumed to occur in the absence of train loading, i.e., under unloaded-track conditions.

The longitudinal displacement of the rail under winter temperature conditions is presented in **Fig. 3**. At the same time, the corresponding axial forces are illustrated in **Fig. 4**. Based on the assumed temperature variations and support conditions applied in the unloaded model, the following results are obtained [26,67]:

- Under winter temperature conditions, the calculated axial force in the rail reaches 224.51 kN within the tunnel section and 1001.67 kN on the open track.
- The corresponding maximum longitudinal displacement is 10.367 mm, occurring at the tunnel portal, where the temperature gradient is the most pronounced.
- For summer conditions, the axial force decreases to 86.35 kN inside the tunnel and 777.15 kN in the open-track section.
- The maximum longitudinal displacement in this case is 8.257 mm, again located at the tunnel entrance.

V. Results Related to the Assumption of p = 7 N/mm

During train loading, the longitudinal resistance of the ballast increases significantly due to vertical forces. In real track conditions, both the longitudinal stiffness and the limiting resistance of the ballast depend on the magnitude of the applied vertical load. Thermal expansion of the rail primarily occurs in unloaded track sections, where ballast resistance is relatively low. These initial displacements are then combined with additional displacements and internal forces in sections where the ballast exhibits greater stiffness and resistance due to train loading.

In the numerical model, however, only a single set of stiffness and resistance parameters can be assigned within a given section. To account for this limitation, a constant longitudinal ballast resistance of p = 7 N/mm was applied along the 300 m track segment subjected to braking. In comparison, a lower value of p = 5 N/mm was assumed for the remaining sections. As a consequence of this simplification, thermal displacements and stresses are also calculated using the higher resistance value within the loaded zone. Due to space limitations, only the main results of the analysis are presented here, without a detailed description of the computational procedure.

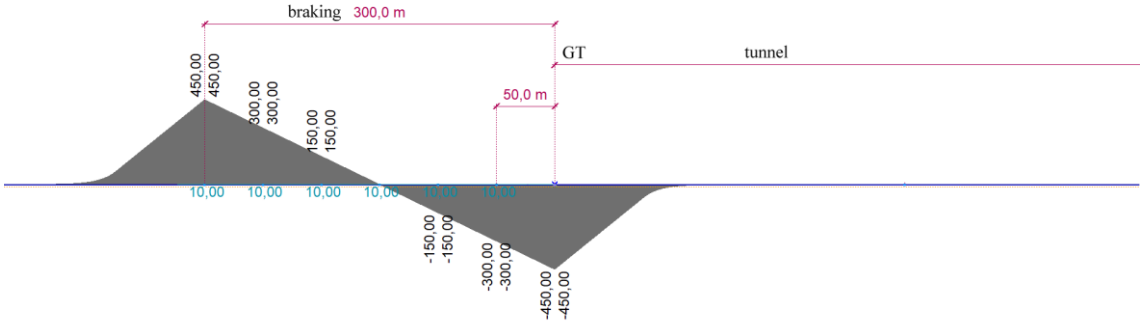

Figure 5. *Normal forces [kN] in the rail due to right (→) braking starting 300 m in front of the gate of the tunnel (decimal commas are applied because of the original AxisVM X5 software)*

When only temperature effects are considered, the maximum longitudinal rail displacement is 8.750 mm in winter and 6.979 mm in summer. In both cases, the largest displacements occur at the tunnel portal, where the temperature gradient is the highest.

When only braking or acceleration forces are applied, without thermal loading, the resulting normal forces in the rail are shown in **Fig. 5** for a braking scenario starting 300 m ahead of the tunnel portal. The distributed braking load is assumed to be 10 kN/m per rail. The longitudinal stiffness of the ballast is assumed to be K = 11.2 kN/mm/m, while the limiting resistance is p = 7 N/mm, which is lower than the applied braking load.

Although such a condition is uncommon in practice, it represents a critical scenario in which the braking force exceeds the available ballast resistance.

In this case, the load applied per unit length exceeds the support's resisting capacity, causing the reaction forces to spread over a distance longer than the 300 m braking length. As a result, significant normal forces develop in the rail, reaching approximately ±450 kN. Compressive forces occur ahead of the braking zone, while tensile forces develop behind it in the direction of braking. In all loading cases, the maximum normal forces occur at the beginning and end of the braking section. In contrast, the maximum longitudinal displacement occurs near the midpoint of the loaded region.

The longitudinal rail displacement corresponding to this loading condition is shown in **Fig. 6** for rightward braking starting 300 m before the tunnel portal. The maximum displacement reaches 36.271 mm and occurs at the center of the braking section.

When the effects of temperature change and braking are considered simultaneously, the highest tensile force in the rail occurs under winter conditions combined with rightward braking starting 300 m in front of the tunnel portal. The maximum tensile force reaches 1389.28 kN and is located at the beginning of the braking section, i.e., 300 m before the tunnel entrance (**Fig. 7**). In general, the extreme values of the normal force are observed at the boundaries of the braking zone, with maximum and minimum forces occurring at the start and end points of the loaded section.

The largest longitudinal rail displacement is 108.425 mm (**Fig. 8**), which occurs under winter temperature conditions combined with leftward braking initiated 150 m before the tunnel, from the open track toward the tunnel. In this loading configuration, the midpoint of the braking section coincides with the tunnel portal.

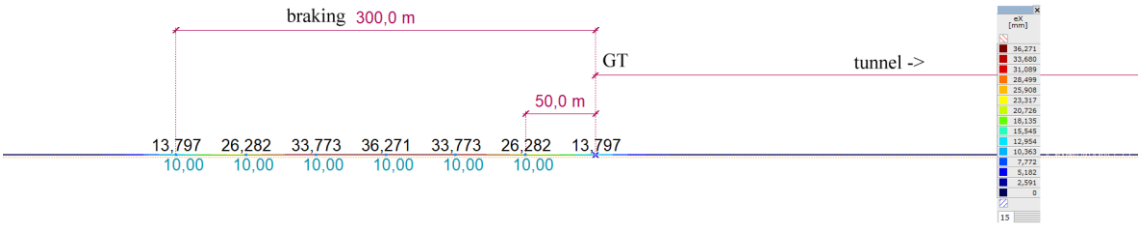

Figure 6. *Longitudinal displacement [mm] of the rail due to right (→) braking starting at 300 m in front of the tunnel, p = 7 N/mm (decimal commas are applied because of the original AxisVM X5 software). The blue markings labeled "10.00" represent the distributed braking load of 10 kN/m applied to a single rail*

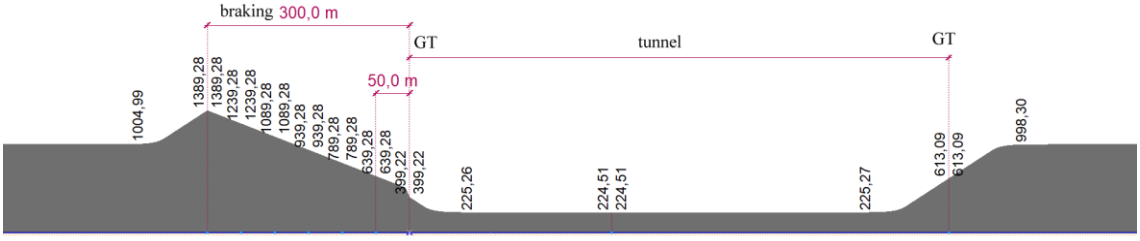

Figure 7. *Normal forces [kN] in the rail due to winter temperature plus right (→) braking starting at 300 m in front of the tunnel, p = 7 N/mm (decimal commas are applied because of the original AxisVM X5 software)*

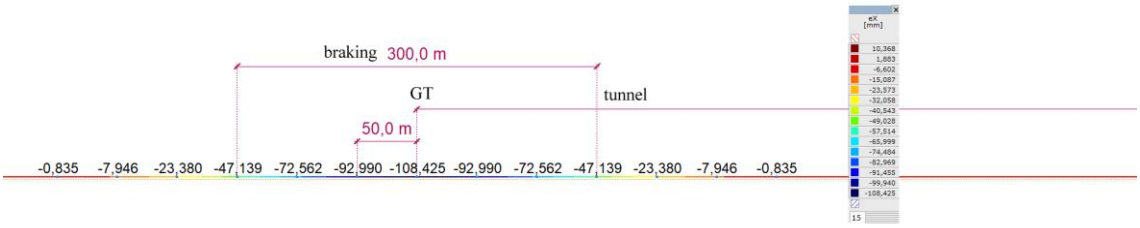

Figure 8. *Displacement [mm] of the rail due to winter temperature plus left (←) braking starting at 150 m in front of the tunnel, p = 7 N/mm (decimal commas are applied because of the original AxisVM X5 software)*

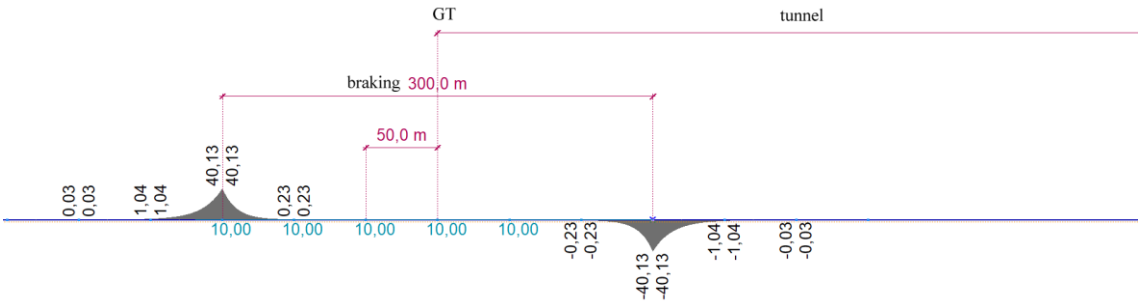

Figure 9. *Normal forces [kN] in the rail due to right (→) braking starting 300 m in front of the gate of the tunnel (decimal commas are applied because of the original AxisVM X5 software). The blue markings labeled "10.00" represent the distributed braking load of 10 kN/m applied to a single rail*

The maximum displacement always develops at the midpoint of the braking zone; therefore, the most critical condition occurs when this midpoint aligns with the abrupt temperature change at the tunnel portal. For comparison, the maximum displacement due to winter temperature change alone is only 7.494 mm in the unloaded model.

The results clearly show that both the normal forces and the longitudinal displacements are significantly higher when thermal effects are combined with braking loads than when temperature effects are considered alone (see Section VII.2). This is particularly evident when the available ballast resistance is lower than the applied braking load. Under such conditions, the track cannot fully resist the imposed forces, leading to substantial increases in both internal forces and rail displacements.

It should be noted that the extremely large displacements obtained in this analysis, on the order of 100 mm, represent a theoretical worst-case scenario. In practice, such conditions are unlikely to occur on well-maintained tracks. For properly compacted and consolidated ballast, the longitudinal resistance under train loading can reach approximately 30 N/mm per rail [5,6], which exceeds the applied braking load of 10 kN/m. Reduced resistance values below 10 N/mm may occur temporarily after ballast renewal or track construction; however, in such cases, operational restrictions, such as reduced speed limits (e.g., 40 km/h), are typically imposed. Further investigation of these transient conditions could be the subject of future research.

VI. Results Related to the Assumption of p = 10 N/mm

When only temperature effects are considered, the maximum longitudinal rail displacement is 7.213 mm in winter and 5.765 mm in summer. In both cases, the largest displacements occur at the

tunnel portal, where the temperature gradient is most pronounced.

When only braking or acceleration loads are applied, without any temperature variation, the resulting rail displacements and normal forces are negligible. In this case, the distributed braking load is taken as 10 kN/m per rail, the longitudinal stiffness of the ballast is K = 16 kN/mm/m, and the limiting resistance is p = 10 N/mm. Under these conditions, the calculated longitudinal displacement is e_x = 0.625 mm. At the boundaries of the braking section, normal forces of approximately 40.13 kN develop in the rail due to the interaction with the adjacent unloaded track sections, where the ballast resistance is p = 5 N/mm. The distribution of normal forces for rightward braking starting 300 m before the tunnel portal is shown in **Fig. 9**.

When the combined effects of temperature variation and braking are considered, the maximum normal force on the rail is 1041.80 kN, which occurs under winter temperature conditions with rightward braking initiated 150 m in front of the tunnel portal (**Fig. 10**). An evaluation of the results shows that including braking does not significantly increase the normal forces compared with those generated by temperature effects alone (see Section IV). This indicates that when the available ballast resistance equals or exceeds the applied braking load, the braking contribution to the overall normal force remains limited.

The maximum longitudinal rail displacement under combined loading is 49.179 mm. This value is obtained for winter temperature conditions combined with leftward braking starting 150 m before the tunnel, from the open track section toward the tunnel. The maximum displacement occurs at the tunnel portal, as illustrated in **Fig. 11**. These results demonstrate that when the ballast resistance equals or exceeds the braking load, the resulting rail displacements are significantly lower than when the resistance is insufficient. For comparison, the displacement due to winter temperature change alone is 5.340 mm in the absence of braking.

VII. EXAMPLES OF THE ELEMENTS OF A DOCUMENT

In this section, a longitudinal ballast resistance of p = 15 N/mm has been assumed for track sections with braking forces, that is, significantly greater than the braking load, and 5 N/mm for other sections.

1. Effects of Temperature Changes Without Braking Force

The longitudinal rail displacements and the corresponding normal forces obtained for the different load cases and load combinations are summarized in Section VII.2. When the model is subjected only to thermal loading (load cases 1 and 2), the maximum rail displacements occur at load

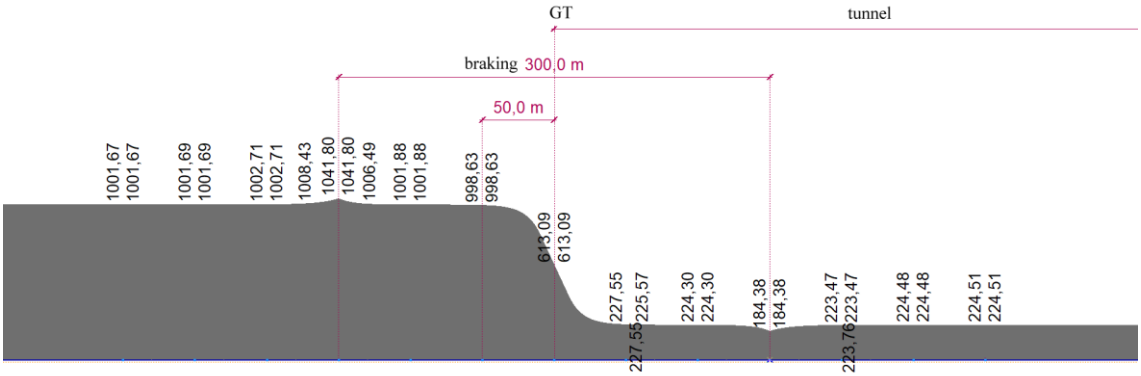

Figure 10. *Normal forces [kN] in the rail due to winter temperature and right braking starting 150 m in front of the gate of the tunnel, p = 10 N/mm (decimal commas are applied because of the original AxisVM X5 software)*

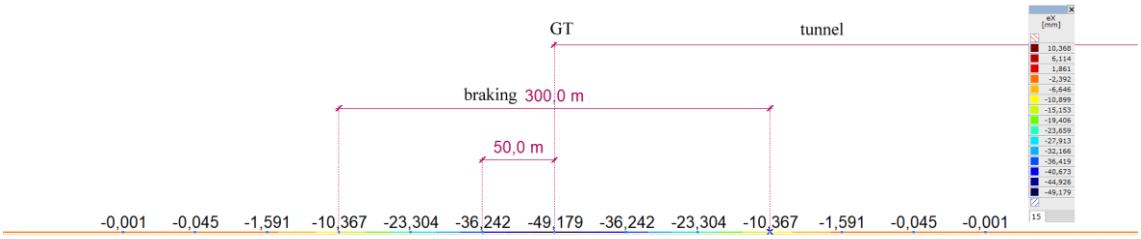

Figure 11. *Longitudinal displacement [mm] of the rail due to winter temperature and left (←) braking starting at 150 m in front of the tunnel, p = 10 N/mm (decimal commas are applied because of the original AxisVM X5 software)*

positions I and VII. The calculated values are 5.701 mm for winter conditions and 4.570 mm for summer conditions. In all cases, the largest temperature-induced displacements are observed at the tunnel portal.

2. Effects of Temperature Changes Without Braking Force

When only braking or acceleration loads are considered, without any temperature variation (load cases 3 and 4 in Table 1), the resulting rail displacements and normal forces are minimal. In this case, the distributed braking load is taken as 10 kN/m per rail, the longitudinal stiffness of the ballast is K = 24 kN/mm/m, and the limiting resistance is p = 15 N/mm. Under these conditions, the calculated longitudinal displacement is e_x = 0.417 mm.

At the boundaries of the braking section, normal forces of approximately 28.95 kN develop in the rail due to the interaction with the adjacent unloaded track, where the ballast resistance is p = 5 N/mm. The distribution of normal forces for rightward braking starting 300 m before the tunnel portal is presented in **Fig. 12**.

A comparison of **Fig. 5**, **Fig. 9**, and **Fig. 12** shows that when the available ballast resistance is equal to or greater than the applied braking load, the resulting normal forces remain relatively small. This indicates that sufficient ballast resistance effectively limits the development of significant longitudinal forces in the rail under braking.

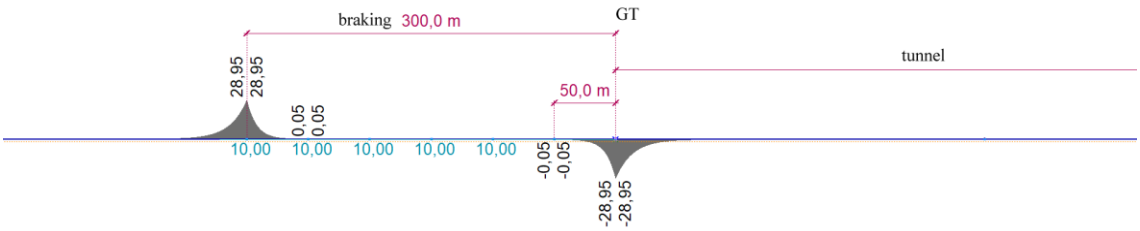

Figure 12. *Normal forces [kN] in the rail due to right braking (→) starting 300 m in front of the gate of the tunnel, p = 15 N/mm (decimal commas are applied because of the original AxisVM X5 software). The blue markings labeled "10.00" represent the distributed braking load of 10 kN/m applied to a single rail*

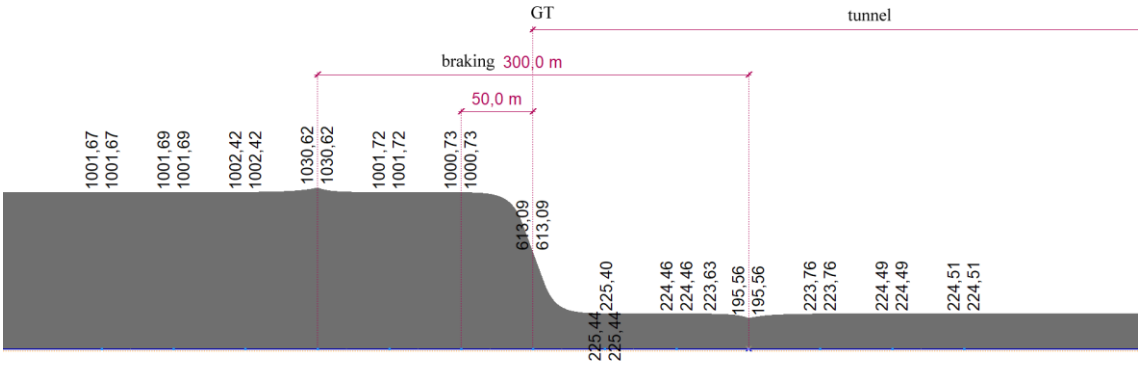

Figure 13. *Normal forces [kN] in the rail due to winter temperature and right (→) braking starting 150 m in front of the gate of the tunnel, p = 15 N/mm (decimal commas are applied because of the original AxisVM X5 software)*

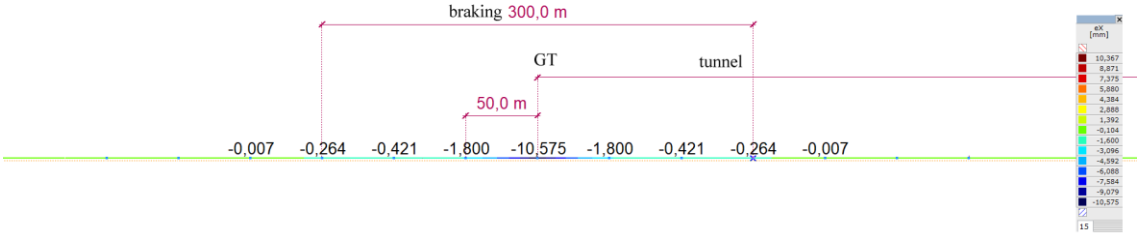

Figure 14. *Longitudinal displacement [mm] of the rail due to winter temperature and left (←) braking starting at 150 m in front of the tunnel, p = 15 N/mm (decimal commas are applied because of the original AxisVM X5 software)*

Table 1. *Maximum values of the rail displacements and the normal forces in the rail resulting from load combinations, p = 15 N/mm on the loaded section (red values are extreme – i.e. governing – values)*

No.	*Load combinations*	*Effects*	*Number of load cases and position of the beginning of the braking in front of the tunnel*						
			I. 300 m	*II. 250 m*	*III. 200 m*	*IV. 150 m*	*V. 100 m*	*VI. 50 m*	*VII. 0 m*
1	winter	displacement e_x [mm]	–5.701	–3.664	–3.664	–3.664	–3.664	–3.664	–5.701
2	summer	displacement e_x [mm]	4.570	2.961	2.961	2.961	2.961	2.961	4.570
3	braking →	displacement e_x [mm]	0.417	0.417	0.417	0.417	0.417	0.417	0.417
		force N [kN]	±28.95	±28.95	±28.95	±28.95	±28.95	±28.95	±28.95
4	braking ←	displacement e_x [mm]	–0.417	–0.417	–0.417	–0.417	–0.417	–0.417	–0.417
		force N [kN]	±28.95	±28.95	±28.95	±28.95	±28.95	±28.95	±28.95
5	winter + braking →	displacement e_x [mm]	–4.010	–2.116	–2.115	–2.115	–2.115	–2.116	–4.010
		force N [kN]	1030.62	1030.62	1030.62	1030.62	1030.62	1029.94	1001.67
6	winter + braking ←	displacement e_x [mm]	–10.471	–10.471	–10.572	–10.575	–10.572	–10.471	–10.471
		force N [kN]	1001.67	1001.67	1001.67	1001.67	1001.67	1001.67	1001.67
7	summer + braking →	displacement e_x [mm]	8.361	8.361	8.464	8.465	8.464	8.361	8.361
		force N [kN]	–777.15	–777.15	–777.15	–777.15	–777.15	–777.15	–777.15
8	winter + braking ←	displacement e_x [mm]	3.204	1.694	1.693	1.693	1.693	1.694	3.204
		force N [kN]	–806.11	–806.11	–806.11	–806.11	–806.11	–805.56	–777.15

3. Effects of the Combination of Change of Temperature and Braking

The longitudinal rail displacements and corresponding normal forces for the different load combinations and load positions – considering both winter and summer temperature conditions as well as leftward and rightward braking – are summarized in **Table 1** (load combinations 5–8).

The maximum normal force on the rail, 1030.62 kN, occurs under winter-temperature conditions combined with rightward braking initiated 150 m in front of the tunnel portal, as shown in **Fig. 13**. An evaluation of the results presented in **Table 1** (load combinations 5–8) indicates that the inclusion of braking loads does not result in a significant increase in normal forces relative to those generated by temperature effects alone (see Section IV).

This behavior is consistent with the findings of the previous section. When the available ballast resistance is greater than or equal to the uniformly distributed braking load, the additional braking effect on the normal forces remains limited. As a result, the combined loading conditions do not produce substantially higher normal forces than those caused by temperature variation alone.

The maximum longitudinal rail displacement is 10.575 mm, which occurs under winter temperature conditions combined with leftward braking starting 150 m in front of the tunnel portal, from the open track section toward the tunnel (load combination 7). The maximum displacement occurs at the tunnel portal, as illustrated in **Fig. 14**.

Under summer temperature conditions combined with braking, the maximum displacement is reduced to 8.465 mm. A comparison of these results with the displacements obtained for temperature loading alone (Section IV) and those summarized in Table 1 (load combinations 5–8) shows that when the ballast resistance is significantly higher than the applied braking load, the additional displacement caused by braking remains limited. In such cases, the total rail displacement is only slightly greater than that resulting from temperature effects alone.

VIII. Conclusions

This study examined the longitudinal behavior of ballasted CWR tracks at tunnel portals, where abrupt changes in thermal conditions occur. A numerical model was developed that incorporates bilinear ballast resistance, experimentally determined fastening properties, and the combined effects of temperature variation and braking loads.

The results clearly show that tunnel portals are critical zones for track performance. The largest rail displacements consistently occur at the portal, where the temperature difference between the open track and the tunnel interior is the greatest. This localized thermal gradient governs the distribution of both longitudinal displacements and axial forces.

The analyses confirm that ballast resistance is the key parameter controlling track behavior. When the available resistance is lower than the applied braking load, very large displacements can develop. In the most unfavorable case, rail movements exceed 100 mm, and axial forces approach 1.4 MN, indicating a potentially unsafe condition. Such situations may occur in practice after maintenance activities or ballast renewal, when resistance is temporarily reduced.

As ballast resistance increases, the track response becomes significantly more stable. When resistance is approximately equal to the braking load, displacements are substantially reduced, and the additional braking effect remains moderate. When the resistance exceeds the braking load, braking forces have only a limited influence, and thermal effects primarily govern track behavior. In this case, the maximum displacements remain relatively small.

The results also show that the interaction between temperature and braking is highly dependent on load position. The most critical condition occurs when the midpoint of the braking zone coincides with the tunnel portal, where the thermal discontinuity is located.

From an engineering perspective, the findings highlight the importance of maintaining adequate ballast resistance, particularly in transition zones. Sections with reduced resistance require special attention, as they are more sensitive to combined thermal and operational loading.

At the same time, the results should be interpreted with caution. The model is based on several simplifying assumptions, including straight track geometry, idealized temperature distributions, and constant resistance values. In reality, temperature changes are gradual, ballast properties vary along the track, and additional factors – such as vehicle-track interaction, residual stresses, and time-dependent effects – also influence track behavior.

Future work should therefore focus on incorporating more realistic temperature fields, variable resistance characteristics, and field measurements for validation. Such developments would improve the reliability of predictions and support a more accurate assessment of track performance at tunnel portals.

Overall, this study provides new insight into the combined effects of thermal loading and braking on CWR tracks and supports improved design and maintenance strategies for railway infrastructure under increasing temperature variations.

Future research should aim to move towards more advanced modeling approaches that combine detailed finite element (FE) simulations with modern data-driven methods [68–73], as well as data analysis with enhanced methodologies [74–77]. While FE models provide a reliable way to describe the thermo-mechanical behavior of railway systems, as shown in recent studies on braking processes and structural performance [68–71], they can be computationally demanding and require well-defined input parameters. In this context, machine learning techniques – especially artificial neural networks – offer a complementary solution, as they can identify complex relationships among loading conditions, material properties, and structural response [72,73]. By combining these two approaches, it would be possible to develop hybrid models that are both accurate and efficient, enabling faster prediction of rail displacements, internal forces, and stability conditions across varying operational scenarios. Such methods could also support parameter optimization and reliability assessment, and may even enable real-time applications in railway infrastructure management. Therefore, future work should focus on integrating FE modeling with neural network techniques to improve both the predictive capability and the practical usability of analyses, particularly in critical transition zones such as tunnel portals.

ACKNOWLEDGEMENT

This paper was prepared with the cooperation of research teams "BME-RAIL" and "SZE-RAIL". This research received no external funding.

AUTHOR CONTRIBUTIONS

N. Liegner: Conceptualization, Methodology, Software, Investigation, Data curation, Writing—original draft preparation, Writing—review and editing, Visualization, Supervision.

S. Fischer: Investigation, Writing—original draft preparation, Writing—review and editing, Supervision.

DISCLOSURE STATEMENT

The authors declare that they have no known competing financial interests or personal relationships that could have appeared to influence the work reported in this paper.

ORCID

N. Liegner http://orcid.org/0009-0008-3368-314X

S. Fischer http://orcid.org/0000-0001-7298-9960

REFERENCES

[1] MÁV Zrt., D.12/H. utasítás: Hézagnélküli felépítmény építése, karbantartása és felügyelete (Instructions of MÁV Zrt. D.12.H of Hungarian State Railways, of construction and maintenance of CWR tracks), KÖZDOK, Budapest, 2009.

[2] E. Nemesdy, Vasúti felépítmény (Railway superstructure), 1st Edition, Tankönyvkiadó, Budapest, 1966.

[3] E. Nemesdy, A hézagnélküli vasúti pályák gátolt dilatációjának pontos és közelítő számítása, valamint a sínvégek illesztésének kialakítása (Accurate and approximative calculation of constrained dilatation of continuously welded rail tracks, and formation of rail joints), Scientific Proceedings of the Technical University of Construction and Transport 5 (2–5) (1960).

[4] EN 1991-2:2003 Eurocode 1: Actions on structures—Part 2: Traffic loads on bridges, ISO Standard (2003).

[5] H. Freystein, M. Muncke, P. Schollmeier, Handbuch Entwerfen von Bahnanlagen (Track installations), 1st Edition, Eurailpress Tetzlaff-Hestra GmbH & Co. KG, Hamburg, 2005.

[6] International Union of Railways (UIC), UIC Code 774-3—Track/bridge interaction: Recommendations for calculations, 2nd Edition, UIC, Paris, 2001.

[7] C. Esveld, Modern Railway Track, 1st Edition, MRT Production, Zaltbommel, 2014.

[8] A. Enshaeian, P. Rizzo, Stability of continuous welded rails: A state-of-the-art review of structural modeling and nondestructive evaluation, Journal of Rail and Rapid Transit 235 (10) (2021) pp. 1291–1311. https://doi.org/10.1177/0954409720986661

[9] N. Mirkovic, L. Brajovic et al., Determination of temperature stresses in CWR based on measured rail surface temperatures, Construction and Building Materials 284 (2021) 122713. https://doi.org/10.1016/j.conbuildmat.2021.122713

[10] L. Chapman, J.E. Thornes, S.P. White, Thermal imaging of railways to identify track sections prone to buckling, Journal of Rail and Rapid Transit 220 (3) (2006) pp. 317–327. https://doi.org/10.1243/09544097JRRT73

[11] M. Ryan, Rail Temperature Measurement Study, AEA Technology Rail, United Kingdom, 2005.

[12] F. Sun, N. Hoult et al., Field monitoring and prediction of the thermal response of an in-service curved continuous welded rail using distributed fiber optic strain measurements, Journal of Civil Structural Health Monitoring (2024). https://doi.org/10.1007/s13349-024-00812-3

[13] G. Liu, H. Liu et al., A new device for stress monitoring in continuously welded rails using bi-directional strain method, Journal of Modern Transportation 26 (3) (2018) pp. 179–188. https://doi.org/10.1007/s40534-018-0164-z

[14] S.S. Ahmad, N.K. Mandal et al., Development of a unified railway track stability management tool to enhance track safety, Journal of Rail and Rapid Transit 227 (5) (2013) pp. 493–516. https://doi.org/10.1177/0954409713501490

[15] A. Skarova, J. Harkness et al., Review of factors affecting stress-free temperature in the continuous welded rail track, Energy Reports 8 (2022) pp. 107–113. https://doi.org/10.1016/j.egyr.2022.11.151

[16] Z. Popović, N. Mirković et al., Temperature stresses in CWR—Experience of Serbian Railways, in: Z. Popovic, A. Manakov, V. Breskich (Eds.), VIII International Scientific Siberian Transport Forum (TransSiberia 2019), Springer, Cham, 2019, pp. 81-102. https://doi.org/10.1007/978-3-030-37916-2_81

[17] R. Kupfer, Auswirkungen von Beschleunigungs- und Bremskräften auf die Längsbewegungen des Gleisrostes, Ph.D. thesis, Technische Universität München (2004). https://mediatum.ub.tum.de/?id=601061

[18] J. Dižo, M. Blatnický et al., Evaluation of ride comfort in a railway passenger car depending on a change of suspension parameters, Sensors 21 (23) (2021) 8138. https://doi.org/10.3390/s21238138

[19] J. Dižo, M. Blatnický et al., Assessment of dynamics of a rail vehicle in terms of running properties while moving on a real track model, Symmetry 14 (3) (2022) 536. https://doi.org/10.3390/sym14030536

[20] J. Soukup, J. Skočilas et al., Vertical vibration of two axle railway vehicle, Procedia Engineering 177 (2017) pp. 25–32. https://doi.org/10.1016/j.proeng.2017.02.179

[21] J. Dižo, M. Blatnický, Use of multibody system dynamics as a tool for rail vehicle behaviour diagnostics, Diagnostyka 17 (2016) pp. 9–16.

[22] I. Taran, R. Olzhabayeva et al., Structural Optimization of Multimodal Routes for Cargo Delivery, Archives of Transport 67 (3) (2023) pp. 49–70. https://doi.org/10.5604/01.3001.0053.7076

[23] I. Taran, G. Bikhimova et al., Improving the Methodology for Optimizing Multimodal Transportation Delivery Routes and Cyclic Schedules in a Transnational Direction, Transport Problems 19 (1) (2024) pp. 157–170. https://doi.org/10.20858/tp.2024.19.1.13

[24] V. Naumov, L. Bekmagambetova et al., Mixed Fuzzy-Logic and Game-Theoretical Approach to Justify Vehicle Models for Servicing the Public Bus Line, Communications – Scientific Letters of the University of Zilina 24 (1) (2022) pp. A26–A34. https://doi.org/10.26552/com.c.2022.1.a26-a34

[25] O. Novytskyi, I. Taran, Z. Zhanbirov, Increasing Mine Train Mass by Means of Improved Efficiency of Service Braking, E3S Web of Conferences 123 (2019) 01034. https://doi.org/10.1051/e3sconf/201912301034

[26] N. Liegner, Determination of rail dilatation movements at tunnel gates for ballasted railway tracks, Periodica Polytechnica Civil Engineering 69 (2) (2025) pp. 644–663. https://doi.org/10.3311/ppci.37989

[27] X. Zhang, W. Broere, Monitoring of tidal variation and temperature change-induced movements of an immersed tunnel using distributed optical fiber sensors (DOFSs), Structural Control and Health Monitoring 2023 (1) (2023) pp. 1–17. https://doi.org/10.1155/2023/2419495

[28] X. Wang, B. Shi et al., Monitoring the behavior of segment joints in a shield tunnel using distributed fiber optic sensors, Structural Control and Health Monitoring 25 (1) (2017) e2056. https://doi.org/10.1002/stc.2056

[29] G. Jing, P. Aela, Review of the lateral resistance of ballasted tracks, Journal of Rail and Rapid Transit 234 (8) (2019) pp. 807–820. https://doi.org/10.1177/0954409719866355

[30] I. Sanchís, R. Insa et al., An analytical model for the prediction of thermal track buckling in dual gauge tracks, Journal of Rail and Rapid Transit 232 (8) (2018) pp. 2163–2172. https://doi.org/10.1177/0954409718764194

[31] P. Piloto, A. Frigeri, M. Minhoto, Thermal buckling of railways, Ce/Papers 5 (2) (2022) pp. 31–40. https://doi.org/10.1002/cepa.1696

[32] D. Agustin, Q. Wu et al., Parallel computing aided analyses of dynamic buckling for railway track infrastructure, Computer-Aided Civil and Infrastructure Engineering 40 (19) (2025) pp. 2943–2968. https://doi.org/10.1111/mice.70004

[33] J. Musazay, A. Zarembski, J. Palese, Determining track-induced lateral thermal expansion forces on a curved railway track, Journal of Rail and Rapid Transit 236 (1) (2021) pp. 3–14. https://doi.org/10.1177/0954409721995318

[34] A. De Iorio, M. Grasso et al., On the ballast–sleeper interaction in the longitudinal and lateral directions, Journal of Rail and Rapid Transit 232 (2) (2018) pp. 620–631. https://doi.org/10.1177/0954409716682629

[35] J. Zakeri, K. Yousefian, Experimental investigation into the longitudinal resistance of ballasted railway track, Journal of Rail and Rapid Transit 235 (8) (2020) pp. 969–983. https://doi.org/10.1177/0954409720975522

[36] M.S. Dersch, M. Potvin et al., Effect of critical factors influencing longitudinal track resistance leveraging laboratory track panel pull test experimentation, Transportation Research Record 2677 (8) (2023) pp. 54–65. https://doi.org/10.1177/03611981231155420

[37] M. Potvin, M. Dersch et al., Review of critical factors influencing longitudinal track resistance, Transportation Research Record 2677 (7) (2023) pp. 558–569. https://doi.org/10.1177/03611981231155170

[38] S. Nobakht, J. Zakeri, A. Safizadeh, Investigation on longitudinal resistance of the ballasted railway track under vertical load, Construction and Building Materials 317 (2022) 126074. https://doi.org/10.1016/j.conbuildmat.2021.126074

[39] A. Safizadeh, J. Zakeri, S. Nobakht, Laboratory investigation on contribution of fastening system and sleeper in longitudinal resistance of ballasted railway tracks, Road Materials and Pavement Design 24 (7) (2022) pp. 1712–1727. https://doi.org/10.1080/14680629.2022.2096104

[40] M. Dersch, M. Potvin et al., Effect of critical factors influencing longitudinal track resistance leveraging field experimentation, Transportation Research Record 2678 (5) (2023) pp. 102–111. https://doi.org/10.1177/03611981231187641

[41] S. Mohammadzadeh, M. Esmaeili, F. Khatibi, A new field investigation on the lateral and longitudinal resistance of ballasted track, Journal of Rail and Rapid Transit 232 (8) (2018) pp. 2138–2148. https://doi.org/10.1177/0954409718764190

[42] M. Alizadeh, M. Imani, J.A. Zakeri, Laboratory and numerical investigation on the longitudinal resistance of ballasted railway tracks with steel sleepers, Construction and Building Materials 402 (2023) 132670. https://doi.org/10.1016/j.conbuildmat.2023.132670

[43] Z. Zeng, C. Tian et al., Experimental study on the longitudinal resistance of WJ-8 fasteners subjected to torque and vertical loading in continuously welded rails, Journal of Rail and Rapid Transit 234 (10) (2019) pp. 1071–1080. https://doi.org/10.1177/0954409719880667

[44] C. Ngamkhanong, B. Feng et al., Evaluation of lateral stability of railway tracks due to ballast

degradation, Construction and Building Materials 278 (2021) 122342. https://doi.org/10.1016/j.conbuildmat.2021.122342

[45] C. Ngamkhanong, S. Kaewunruen, C. Baniotopoulos, Influences of ballast degradation on railway track buckling, Engineering Failure Analysis 122 (2021) 105252. https://doi.org/10.1016/j.engfailanal.2021.105252

[46] C. Shi, Y. Zhou et al., A critical review on the vertical stiffness irregularity of railway ballasted track, Construction and Building Materials 400 (2023) 132715. https://doi.org/10.1016/j.conbuildmat.2023.132715

[47] O. Javaid, D. Choi, Effect of track irregularities on the response of two-way railway tracks, Applied Sciences 10 (1) (2020) 4216. https://doi.org/10.3390/app10010011

[48] Y. Tong, G. Liu et al., Track vertical stiffness—Value, measurement methods, effective parameters and challenges: A review, Transportation Geotechnics 37 (2022) 100833. https://doi.org/10.1016/j.trgeo.2022.100833

[49] B. Indraratna, Y. Qi et al., Recycled materials in railroad substructure: An energy perspective, Railway Engineering Science 30 (3) (2022) pp. 304–322. https://doi.org/10.1007/s40534-021-00267-6

[50] S. Fischer, D. Harangozó et al., Investigation of heat-affected zones of thermite rail weldings, Facta Universitatis, Series: Mechanical Engineering 22 (4) (2024) pp. 689–710. https://doi.org/10.22190/FUME221217008F

[51] V. Tertychnyi, G. Vatulia et al., Determination of the primary technical parameters of the test bench for controlling the temperature of rails and rail bars of continuous welded rail, MATEC Web of Conferences 133 (2017) 03002. https://doi.org/10.1051/matecconf/201713303002

[52] G. Bianchi, C. Fanelli et al., Systematic review railway infrastructure monitoring: From classic techniques to predictive maintenance, Advances in Mechanical Engineering 17 (1) (2025). https://doi.org/10.1177/16878132241285631

[53] A. Consilvio, M. Iorani et al., Real-time monitoring of the longitudinal strain of continuous welded rail for safety improvement, Journal of Rail and Rapid Transit 234 (10) (2019) pp. 1238–1252. https://doi.org/10.1177/0954409719890166

[54] K. Izotov, D. Loktev et al., Determination of rail deformations using fiber optic technologies, E3S Web of Conferences 389 (2023) 05045. https://doi.org/10.1051/e3sconf/202338905045

[55] M. Vagnoli, R. Remenyte-Prescott, An ensemble-based change-point detection method for identifying unexpected behaviour of railway tunnel infrastructures, Tunnelling and Underground Space Technology 81 (2018) pp. 68–82. https://doi.org/10.1016/j.tust.2018.07.013

[56] A. MacDonald, J. McDonald et al., New York State Climate Impacts Assessment Chapter 09: Transportation, Annals of the New York Academy of Sciences 1542 (2024) pp. 501–560. https://doi.org/10.1111/nyas.15198

[57] S. Tamagawa, Y. Nishinomiya et al., Effects of ballast renewal work at low temperature on inward rail displacements and axial rail forces of continuous welded rails on sharp curve, Transactions of the JSME 86 (889) (2020) 20-00244. https://doi.org/10.1299/transjsme.20-00244

[58] R. Wang, G. Jing et al., Under ballast mat—A review of recent developments, limitations, and future prospects, Journal of Rail and Rapid Transit 237 (8) (2023) pp. 983–995. https://doi.org/10.1177/09544097221150494

[59] S. Kaewunruen, C. Ngamkhanong et al., Wet/dry influence on behaviors of closed-cell polymeric cross-linked foams under static, dynamic and impact loads, Construction and Building Materials 187 (2018) pp. 1092–1102. https://doi.org/10.1016/j.conbuildmat.2018.08.052

[60] B. Indraratna, Y. Qi et al., Advances in ground improvement using waste materials for transportation infrastructure, Proceedings of the Institution of Civil Engineers—Ground Improvement 175 (1) (2022) pp. 3–22. https://doi.org/10.1680/jgrim.20.00007

[61] G. Jing, L. Qie et al., Polyurethane reinforced ballasted track: Review, innovation and challenge, Construction and Building Materials 208 (2019) pp. 734–748. https://doi.org/10.1016/j.conbuildmat.2019.03.031

[62] L. Ézsiás, R. Tompa, S. Fischer, Investigation of the possible correlations between specific characteristics of crushed stone aggregates, Spectrum of Mechanical Engineering and Operational Research 1 (1) (2024) pp. 10–26. https://doi.org/10.31181/smeor1120242

[63] S. Fischer, Investigation of the settlement behavior of ballasted railway tracks due to dynamic loading, Spectrum of Mechanical Engineering and Operational Research 2 (1) (2025) pp. 24–46. https://doi.org/10.31181/smeor21202528

[64] S. Fischer, S. Kocsis Szürke, Detection process of energy loss in electric railway vehicles,

Facta Universitatis, Series: Mechanical Engineering 21 (1) (2023) pp. 81–99. https://doi.org/10.22190/FUME221104046F

[65] EN 13146-1:2019 Railway applications—Track—Test methods for fastening systems—Part 1: Determination of longitudinal rail restraint, ISO Standard (2019).

[66] H. Papp, N. Liegner, Investigation of internal forces in the rail due to the interaction of CWR tracks and steel bridges with ballasted track superstructure, Pollack Periodica 11 (2) (2016) pp. 65–74. https://doi.org/10.1556/606.2016.11.2.6

[67] N. Liegner, Alagutak kapuzatainál kialakuló síndilatációs mozgások (Rail dilatation movements at gates of tunnels), Sínek Világa 63 (4–5) (2021) pp. 54–59.

[68] B. Bolló, F. Sarka et al., Thermal Analysis of a Simplified Railway Brake Model with Numerical Simulation, Periodica Polytechnica Transportation Engineering 53 (1) (2025) pp. 1–6. https://doi.org/10.3311/PPtr.36938

[69] A. Lovska, J. Gerlici et al., Strength Analysis of Sectional Flat Wagon Supporting Structures When Transported by a Railway Ferry, Acta Technica Jaurinensis 18 (1) (2025) pp. 46–53. https://doi.org/10.14513/actatechjaur.00876

[70] A.T.J. Kuchak, D. Marinkovic, M. Zehn, Finite Element Model Updating—Case Study of a Rail Damper, Structural Engineering and Mechanics 73 (1) (2020) pp. 27–35. https://doi.org/10.12989/sem.2020.73.1.027

[71] A.J.T. Kuchak, D. Marinkovic, M. Zehn, Parametric Investigation of a Rail Damper Design Based on a Lab-Scaled Model, Journal of Vibration Engineering & Technologies 9 (1) (2021) pp. 51–60. https://doi.org/10.1007/s42417-020-00209-2

[72] F. Nikolić, M. Čanađija, Machine Learning of Structure–Property Relationships: An Application to Heat Generation during Plastic Deformation, Facta Universitatis, Series: Mechanical Engineering 23 (4) (2025) pp. 687–707. https://doi.org/10.22190/FUME240201040N

[73] J. Gokulachandran, M. Thenarasu et al., Reliability Prediction and Process Parameter Optimization of Welded Joints: Artificial Neural Network and Fuzzy Logic, Facta Universitatis, Series: Mechanical Engineering 23 (4) (2025) pp. 945–969. https://doi.org/10.22190/FUME240214055G

[74] M.M. Zefreh, M.A. Saif et al., A data-driven decision support tool for public transport service analysis and provision, Transport Policy 135 (2023) pp. 82–90. https://doi.org/10.1016/j.tranpol.2023.01.015

[75] M. Lekić, K. Rogić et al., Big data in logistics, Periodica Polytechnica Transportation Engineering 49 (1) (2021) pp. 60–65. https://doi.org/10.3311/PPtr.14589

[76] D. Tollner, M. Zöldy, Road Type Classification of Driving Data Using Neural Networks, Computers 14 (2) (2025) 70. https://doi.org/10.3390/computers14020070

[77] O. Orynycz, P. Ruchała et al., A theoretical analysis of meteorological data as a road towards optimizing wind energy generation, Energies 17 (11) (2024) 2765. https://doi.org/10.3390/en17112765